Research Article | Vol. 24, No. 15 | 25 Jul 2016 | OPTICS EXPRESS 16894

Optics EXPRESS

Light absorption enhancement in Ge nanomembrane and its optoelectronic application

MUNHO KIM,[1,3] SHIH-CHIA LIU,[2] TONG JUNE KIM,[1] JAESEONG LEE,[1] JUNG-HUN SEO,[1] WEIDONG ZHOU,[2,*] AND ZHENQIANG MA[1,*]

[1]*Department of Electrical and Computer Engineering, University of Wisconsin at Madison, Madison, WI 53706, USA*
[2]*Department of Electrical Engineering, University of Texas at Arlington, Arlington, TX 76019, USA*
[3]*Current address: Department of Electrical and Computer Engineering, University of Illinois at Urbana-Champaign, Urbana, IL 61801, USA*
[4]*wzhou@uta.edu*
[5]*mazq@engr.wisc.edu*

Abstract: In this study, the light absorption property of Ge nanomembrane (Ge NM), which incorporates hydrogen (H), in near-infrared (NIR) wavelength range was analyzed. Due to the presence of a large amount of structural defects, the light absorption coefficient of the Ge layer becomes much higher (10 times) than that of bulk Ge in the wavelength range of 1000 ~1600 nm. Increased light absorption was further measured from released Ge NM that has H incorporation in comparison to that of bulk Ge, proving the enhanced light absorption coefficient of H incorporated Ge. Finally, metal-semiconductor-metal (MSM) photodetectors were demonstrated using the H incorporated Ge on GeOI.

OCIS codes: (310.6860) Thin films, optical properties; (160.1890) Detector materials; (160.6000) Semiconductor materials; (230.0040) Detectors.

References and links

1. R. Soref, "Mid-infrared photonics in silicon and germanium," Nat. Photonics **4**(8), 495–497 (2010).
2. W. C. Dash and R. Newman, "Newman, R. Intrinsic optical absorption in single-crystal germanium and silicon at 77°K and 300°K," Phys. Rev. **99**(4), 1151–1155 (1955).
3. S. V. Kartalopoulos, "Elastic bandwidth [optical-fiber communication]," IEEE Circuits Dev. Mag. **18**(1), 8–13 (2002).
4. C. A. Brackett, "Dense wavelength division multiplexing networks: principles and applications," IEEE J. Sel. Areas Comm. **8**(6), 948–964 (1990).
5. E. D. Palik, *Handbook of Optical Constants of Solids* (Academic, 1985).
6. S. Su, B. Cheng, C. Xue, W. Wang, Q. Cao, H. Xue, W. Hu, G. Zhang, Y. Zuo, and Q. Wang, "GeSn p-i-n photodetector for all telecommunication bands detection," Opt. Express **19**(7), 6400–6405 (2011).
7. J. Liu, D. D. Cannon, K. Wada, Y. Ishikawa, S. Jongthammanurak, D. T. Danielson, J. Michel, and L. C. Kimerling, "Tensile strained Ge photodetectors on Si platform for C and L band telecommunications," Appl. Phys. Lett. **87**(1), 011110 (2005).
8. Z. Xia, H. Song, M. Kim, M. Zhou, T.-H. Chang, D. Liu, K. Xiong, Z. Yu, Z. Ma, and Q. Gan, "Photodetecting MOSFET based on ultrathin single-crystal germanium nanomembrane," in *Conference on Lasers and Electro-Optics, OSA Conference Papers* (Optical Society of America, 2016), paper STh4E.
9. M. Cho, J.-H. Seo, M. Kim, J. Lee, D. Liu, W. Zhou, Z. Yu, and Z. Ma, "Resonant cavity germanium photodetector via stacked single-crystalline nanomembranes," J. Vac. Sci. Technol. B **34**(4), 040604 (2016).
10. J. R. Sánchez-Pérez, C. Boztug, F. Chen, F. F. Sudradjat, D. M. Paskiewicz, R. B. Jacobson, M. G. Lagally, and R. Paiella, "Direct-bandgap light-emitting germanium in tensilely strained nanomembranes," Proc. Natl. Acad. Sci. U.S.A. **108**(47), 18893–18898 (2011).
11. J. Liu, X. Sun, L. C. Kimerling, and J. Michel, "Direct-gap optical gain of Ge on Si at room temperature," Opt. Lett. **34**(11), 1738–1740 (2009).
12. H.-C. Yuan, J. Shin, G. Qin, L. Sun, P. Bhattacharya, M. G. Lagally, G. K. Celler, and Z. Ma, "Flexible photodetectors on plastic substrates by use of printing transferred single-crystal germanium membranes," Appl. Phys. Lett. **94**(1), 013102 (2009).
13. J. R. Jain, A. Hryciw, T. M. Baer, D. A. B. Miller, M. L. Brongersma, and R. T. Howe, "A micromachining-based technology for enhancing germanium light emission via tensile strain," Nat. Photonics **6**(5), 398–405 (2012).
14. W. S. Ho, Y.-H. Dai, Y. Deng, C.-H. Lin, Y.-Y. Chen, C.-H. Lee, and C. W. Liu, "Flexible Ge-on-polyimide detectors," Appl. Phys. Lett. **94**(26), 261107 (2009).

#265152 http://dx.doi.org/10.1364/OE.24.016891
Journal © 2016 Received 13 May 2016; revised 24 Jun 2016; accepted 13 Jul 2016; published 18 Jul 2016
Corrected: 5 August 2016

Optics EXPRESS

15. C. J. Tracy, P. Fejes, N. D. Theodore, P. Maniar, E. Johnson, A. J. Lamm, A. M. Paler, I. J. Malik, and P. Ong, "Germanium-on-insulator substrates by wafer bonding," J. Electron. Mater. **33**(8), 886–892 (2004).
16. J. M. Zahler, A. Fontcuberta i Morral, M. J. Griggs, H. A. Atwater, and Y. J. Chabal, "Role of hydrogen in hydrogen-induced layer exfoliation of germanium," Phys. Rev. B **75**(1), 035309 (2007).
17. Y.-L. Chao, R. Scholz, M. Reiche, U. Gosele, and J. C. S. Woo, "Characteristics of germanium-on-insulators fabricated by wafer bonding and hydrogen-induced layer splitting," Jpn. J. Appl. Phys. **45**(11), 8565–8570 (2006).
18. J.-H. Seo, K. Zhang, M. Kim, D. Zhao, H. Yang, W. Zhou, and Z. Ma, "Flexible Phototransistors Based on Single-Crystalline Silicon Nanomembranes," Adv. Opt. Mater. **4**(1), 120–125 (2016).
19. A. H. Kahn, "Theory of the infrared absorption of carriers in germanium and silicon," Phys. Rev. **97**(6), 1647–1652 (1955).
20. V. Sorianello, L. Colace, N. Armani, F. Ross, C. Ferrari, L. Lazzarini, and G. Assanto, "Low-temperature germanium thin films on silicon," Opt. Mater. Express **1**(5), 856–865 (2011).
21. J. M. Zavada, H. A. Jenkinson, R. G. Sarkis, and R. G. Wilson, "Hydrogen depth profiles and optical characterization of annealed, proton-implanted n-type GaAs," J. Appl. Phys. **58**(10), 3731–3734 (1985).
22. I. P. Ferain, K. Y. Byun, C. A. Colinge, S. Brightup, and M. S. Goorsky, "Low temperature exfoliation process in hydrogen-implanted germanium layers," J. Appl. Phys. **107**(5), 054315 (2010).
23. F. Fournel, H. Moriceau, and R. Beneyton, "Low temperature void free hydrophilic or hydrophobic silicon direct bonding," ECS Trans. **3**(6), 139–146 (2006).
24. K. Zhang, J.-H. Seo, W. Zhou, and Z. Ma, "Fast flexible electronics using transferrable silicon nanomembranes," J. Phys. D Appl. Phys. **45**(14), 143001 (2012).
25. T. Akatsu, C. Deguet, L. Sanchez, F. Allibert, D. Rouchon, T. Signamarcheix, C. Richtarch, A. Boussagol, V. Loup, F. Mazen, J.-M. Hartmann, Y. Campidelli, L. Clavelier, F. Letertre, N. Kernevez, and C. Mazure, "Germanium-on-insulator (GeOI) substrates-A novel engineered substrate for future high performance devices," Mater. Sci. Semicond. Process. **9**(4–5), 444–448 (2006).
26. D. K. Schroder, *Semiconductor Material and Device Characterization* (John Wiley and Sons, 1990).
27. P. D. Townsend, L. Zhang, and P. J. Chandler, *Optical Effects of Ion Implantation* (Cambridege University, 1994).
28. A. G. Foyt, W. T. Lindley, C. M. Wolfe, and J. P. Donnelly, "Isolation of junction devices in GaAs using proton bombardment," Solid-State Electron. **12**(4), 209–214 (1969).
29. E. Garmire, H. Stoll, A. Yariv, and R. G. Hunsperger, "Optical waveguiding in proton-implanted GaAs," Appl. Phys. Lett. **21**(3), 87–88 (1972).
30. J. P. van der Ziel, W. T. Tsang, R. A. Logan, and W. M. Augustyniak, "Subpicosecond pulses from passively mode-locked GaAs buried optical guide semiconductor lasers," Appl. Phys. Lett. **39**(7), 525–527 (1981).
31. S. J. Pearton, J. W. Corbett, and T. S. Shi, "Hydrogen in crystalline semiconductors," Appl. Phys., A Mater. Sci. Process. **43**(3), 135–195 (1987).
32. J.A. Woollam Co, "WVASE," https://www.jawoollam.com/ellipsometry-software/wvase
33. H. R. Philipp and E. A. Taft, "Optical Constants of Germanium in the Region 1 to 10 ev," Phys. Rev. **113**(4), 1002–1005 (1959).
34. R. A. Soref and B. R. Bennett, "Electrooptical effects in silicon," IEEE J. Quantum Electron. **23**(1), 123–129 (1987).
35. J. Michel, J. Liu, and L. C. Kimerling, "High-performance Ge-on-Si photodetectors," Nat. Photonics **4**(7), 527–534 (2010).
36. E. D. Capron and O. L. Brill, "Absorption coefficient as a function of resistance for optical germanium at 10.6 μm," Appl. Opt. **12**(3), 569–572 (1973).
37. S. Logothetidis, "Polymeric substrates and encapsulation for flexible electronics: bonding structure, surface modification and functional nanolayer growth," Rev. Adv. Mater. Sci. **10**(5), 387–397 (2005).
38. P. W. Kruse, L. D. McGlauchlin, and R. B. McQuistan, *Elements of Infrared Technology* (John Wiley and Sons, 1962).
39. J. L. Digaum, J. J. Pazos, J. Chiles, J. D'Archangel, G. Padilla, A. Tatulian, R. C. Rumpf, S. Fathpour, G. D. Boreman, and S. M. Kuebler, "Tight control of light beams in photonic crystals with spatially-variant lattice orientation," Opt. Express **22**(21), 25788–25804 (2014).
40. J. F. Elman, J. Greener, C. M. Herzinger, and B. Johs, "Characterization of biaxially-stretched plastic films by generalized ellipsometry," Thin Solid Films **313–314**(2), 814–818 (1998).
41. A. K. Okyay, A. M. Nayfeh, K. C. Saraswat, T. Yonehara, A. Marshall, and P. C. McIntyre, "High-efficiency metal-semiconductor-metal photodetectors on heteroepitaxially grown Ge on Si," Opt. Lett. **31**(17), 2565–2567 (2006).

1. Introduction

Germanium (Ge) has been a key semiconductor material in photonic and optoelectronic applications in the NIR wavelength range due to its superior light absorption property [1,2]. Especially, the wavelengths beyond 1.55 μm are critically important because the wavelength range for the dense wavelength division multiplexing (DWDM) technology expands to L-band (i.e., 1561 ~1620 nm) [3,4]. However, Ge photodetectors typically suffer from low responsivity at wavelengths longer than 1.55 μm due to the abrupt drop in its absorption

Optics EXPRESS

coefficient that begins at ~1.5 μm [5]. Therefore, strategies to improve the Ge light absorption beyond 1.55 μm have been sought and intensive research has been carried out to enhance the absorption of Ge in the NIR wavelength range [6,7].

In recent years, Ge nanomembrane (Ge NM), which has a thickness that ranges from several tens of nanometers [8] to hundreds of nanometers [9], exhibited its importance in optoelectronic applications. Ge based infrared optical gain media and flexible Ge photodetectors have been demonstrated [10–12]. The Ge on insulator (GeOI) wafers, which are the source materials of Ge NMs, have been created either by using epitaxy growth (e.g., on top of a temporary/sacrificial GaAs substrate) or a Smart-Cut® process (the most widely used) [13,14]. In the Smart-Cut® process, hydrogen (H) ion implantation is used to split the transferrable thin Ge layers from the bulk Ge wafer [15]. Annealing the H implanted Ge wafer induces the exfoliation of the Ge layer from bulk Ge wafer [16]. The damaged Ge layer by implanted H ions can be mostly removed by the subsequent chemical mechanical planarization (CMP) process. However, it is reported that high concentrations of vacancies in the order of 10^{21} /cm^3 can be created in Ge during ion implantation [17]. Residual H ions still exist inside the Ge layer, with a concentration range of 10^{19} ~10^{20} /cm^3 [17]. Although a thicker (like bulk) Ge layer has the advantage of better light absorption, a thinner Ge layer (e.g., Ge NM) has more flexibility on the device fabrication [9,18]. Regardless of the thickness, the light absorption coefficient of Ge (i.e., both bulk Ge and Ge NM) decreases rapidly at wavelengths longer than 1.5 μm [5]. Therefore, it is desirable to enhance the light absorption coefficient of Ge so that the total light absorption can be greatly enhanced in Ge-based optical sensor applications for both long haul and on-chip optical communications.

In this paper, we report a thorough analysis of light absorption of the Ge NM associated with H ion implantation. The optical properties of H-implanted Ge layer in GeOI wafers were characterized and it was found that the refractive index and the extinction coefficient can be manipulated by H implantation. In general, light absorption of semiconductor material increases with higher doping concentration and structural defects [19,20]. Previously, it was reported that the optical properties of GaAs were modified by H implantation [21]. Here, GeOI and Ge NMs have been studied with the evidence that implanted H ions might be the reason for the improvements, which needs to be further investigated. The enhanced light absorption of H implanted Ge was further confirmed by investigating the responsivity of metal-semiconductor-metal (MSM) photodetectors that are fabricated using the H-implanted Ge NM.

2. Experiment

Figure 1 shows the fabrication process flow of the GeOI wafers. The process began with an unintentionally doped 4-inch intrinsic bulk Ge wafer with a resistivity larger than 40 Ω-cm [Fig. 1(a)]. A 100 nm thick plasma enhanced chemical vapor deposition (PECVD) SiO_2 layer was deposited on the Ge wafers as a screen oxide in order to obtain a uniform ion implantation profile [22]. The oxide-capped Ge wafers were implanted by H + ions with a dose of 1×10^{17} cm^{-2} and an energy of 100 keV [Fig. 1(b)]. The peak position of the hydrogen implantation profile was carefully designed to be placed at 700 nm from the Ge surface in order to acquire a 400 nm thick Ge layer after the splitting process. A 200 nm thick SiO_2 was grown on a Si handling substrate as the buried oxide (BOX) layer for the final structure of the GeOI. Prior to the wafer bonding between the H implanted Ge wafers and the oxidized Si substrate, the PECVD SiO_2 was removed from the Ge substrate using concentrated hydrofluoric acid (HF, 49%) and an oxygen plasma activation process on a SiO_2/Si substrate was carried out to enhance the bonding strength. The wafer bonding process was performed using a direct wafer bonder (EV 801) under a vacuum of 7×10^{-5} mbar [Fig. 1(c)]. After finishing physical contact between the H implanted Ge wafer and the SiO_2/Si wafer in the wafer bonder, a careful temperature control during the annealing step with a ramp up/down of 1˚C/min was applied to avoid fracture of bonded wafers due to their different coefficients of thermal expansion [23]. In addition to the annealing process in the wafer bonder, a two-step, low temperature annealing at 200˚C and 250˚C were carried out in a

Optics EXPRESS

nitrogen-filled oven to improve the nucleation of hydrogen platelets to achieve a complete separation of the Ge layer from the Ge bulk substrate [Figs. 1(d)-1(e)]. A ~700 nm thick Ge layer with the rough surface facing up was successfully transferred onto the SiO_2/Si handling wafer without any visible voids. The rough Ge surface, which has a root mean square (RMS) value (R_q) of 22 nm, was polished down to 0.5 nm, giving a final Ge thickness of about 400 nm [Fig. 1(e)].

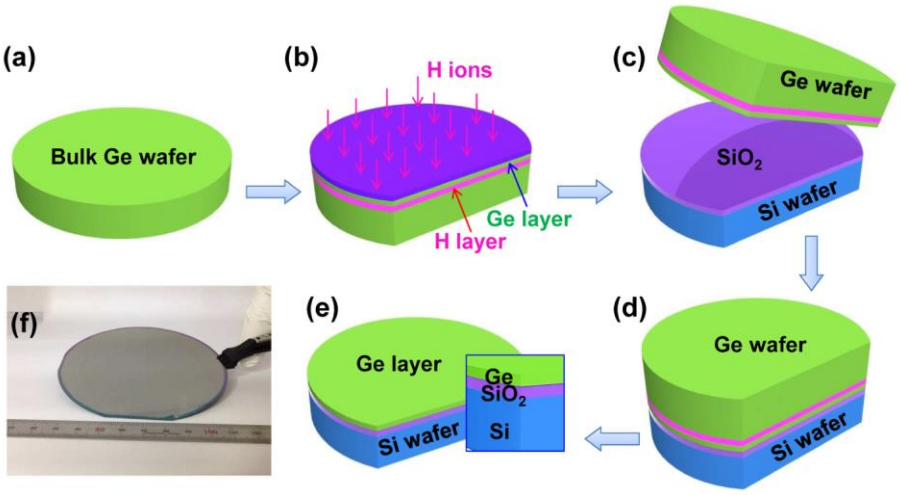

Fig. 1. A schematic process flow of the fabrication of GeOI wafer: (a) Cleaning a bulk Ge wafer. (b) Depositing a 100 nm thick PECVD SiO_2 layer on top of the Ge wafer followed by hydrogen implantation. (c) Wafer bonding to thermally oxidized Si handling wafer. (d) Annealing the bonded wafers for splitting Ge layers by hydrogen exfoliation. (e) Polishing a transferred Ge layer to the desired thickness to achieve a smooth surface roughness. (f) An optical image of the fabricated GeOI wafer.

To investigate the effect of thermal annealing on the electrical and optical properties of Ge layer, the finished GeOI wafer was annealed using rapid thermal annealing (RTA) at 600˚C for 3 minutes in nitrogen ambient. Transfer length measurements (TLM) were carried out on as-fabricated (non-annealed: NA) and annealed (A) GeOI wafers with three different thicknesses of Ge layers (i.e., 400, 175, and 50 nm) to quantify the free-carrier concentrations inside the Ge layer.

To characterize the optical properties of the Ge layer of the GeOI wafer, the Ge layer was released from the GeOI wafer and transferred onto a transparent plastic substrate. The detailed process can be found elsewhere [24]. In short, the top Ge layer was patterned and undercut in HF (49%) solution to remove the BOX layer. The released top Ge layer, now called the Ge NM, was flip-transferred onto a 1 μm thick adhesive layer (Microchem, SU-8 2002) coated on 180 μm thick polyethylene terephthalate (PET) film. Transferred Ge NMs (size: 5 × 5 mm^2) were completely glued to the PET films by a UV curing process. The Ge NM reflection and transmission spectra were measured at room temperature. A light source (Ocean Optics, HL-2000) was used and the light went through the fiber, collimator, aperture, and × 4 objective lens. Both the reflection and the transmission were measured from surface normal incidence which has a spectral range of 1000 ~1600 nm. The spectra were collected using two fiber coupling adapters that were connected to an optical spectrum analyzer (Yokogawa, AQ6370B), simultaneously.

Finally, MSM photodetectors were fabricated on non-annealed and annealed GeOI wafers to illustrate the improved photo responsivity of the H incorporated Ge layer. Interdigitated metal electrodes (Ti/Au = 50/450 nm) with a 2 μm width and a 6 μm distance between the electrodes were e-beam evaporated on the 40 × 70 μm^2 patterned Ge layer, followed by the deposition of a 250 nm thick PECVD SiO_2 layer and the opening of the contact windows. I-V characteristics of the fabricated devices were measured using a semiconductor parameter

Optics EXPRESS

analyzer (HP4155B) under dark and illuminated conditions. Infrared light at wavelengths of 1.5, 1.55, 1.6, and 1.64 μm was focused on the device via a lensed fiber with incident powers of 70, 125, 180, and 200 μW, respectively.

3. Results and discussion

Figure 1(f) shows an optical image of a finished 4-inch GeOI wafer and its corresponding cross-sectional scanning electron microscopy (SEM) image is shown in Fig. 2(a), for which the buried interfaces after annealing at 250 °C for 1 hour and the subsequent CMP process were applied. The thicknesses of the Ge layer and the BOX layer were measured to be 400 and 200 nm, respectively. These values corresponded well with our target layer thicknesses.

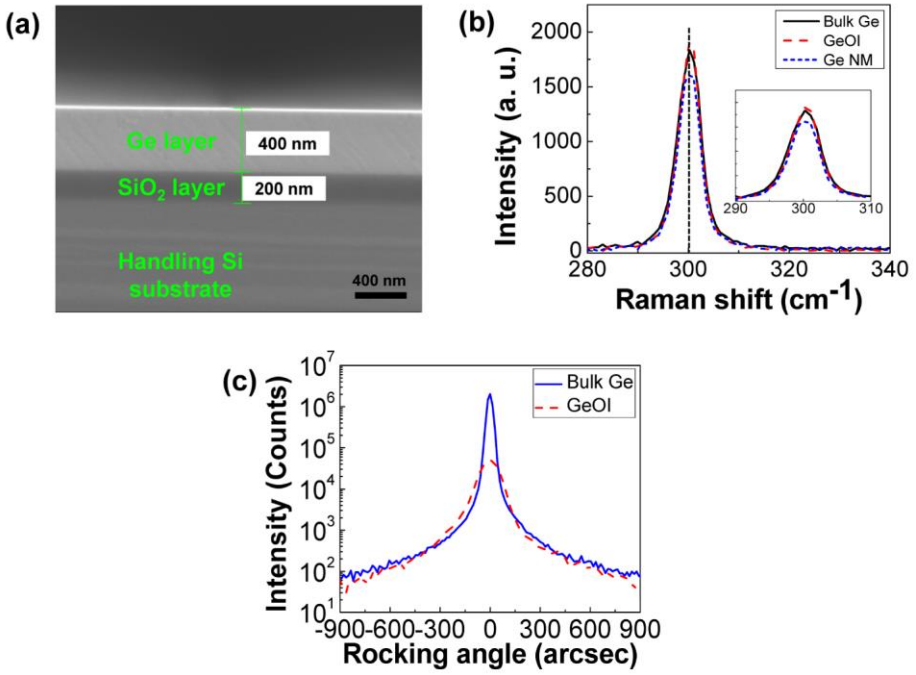

Fig. 2. (a) A cross-sectional SEM image of the GeOI wafer. (b) Measured Raman spectra from bulk Ge wafer, GeOI wafer, and Ge NM on PET substrate, respectively. (c) HR-XRD rocking curves of the bulk Ge and GeOI.

It is important to note the crystallinity and the residual strain of the Ge layer in the fabricated GeOI wafer, since the process for the GeOI wafer fabrication involves several steps of thermal processes with high pressure. Horiba LabRAM ARAMIS Raman spectroscopy with a green laser (532 nm) was used to investigate the material properties from the top surface of the Ge layer. Spectral resolution is 0.01 cm^{-1}. Figure 2(b) shows a comparison of the Raman spectrum taken from a bulk Ge wafer, the Ge layer in our fabricated GeOI wafer, and the as-transferred Ge NM on PET substrate, respectively. The bulk Ge wafer was used as the reference, which has a Ge-Ge characteristic peak at 300.29 cm^{-1} [25]. The same 300.29 cm^{-1} Ge-Ge characteristic peaks from other two cases (i.e., the Ge layer in GeOI wafer and as-transferred Ge NM on PET substrate) confirmed that no strain was introduced in the Ge layer of the GeOI wafer or in the released and transferred Ge NM. We investigated full width at half maximum (FWHM) of the bulk Ge and GeOI using high resolution X-ray diffraction (HR-XRD, PANalytical X'Pert PRO XRD). Rocking curves of both samples were scanned around the (004) reflection as shown in Fig. 2(c). The FWHM of the bulk Ge was measured to be 43 arcsec, while it increased to 124 arcsec measured from the GeOI. The increased FWHM was probably caused by the structural defects associated with H ion implantation.

Optics EXPRESS

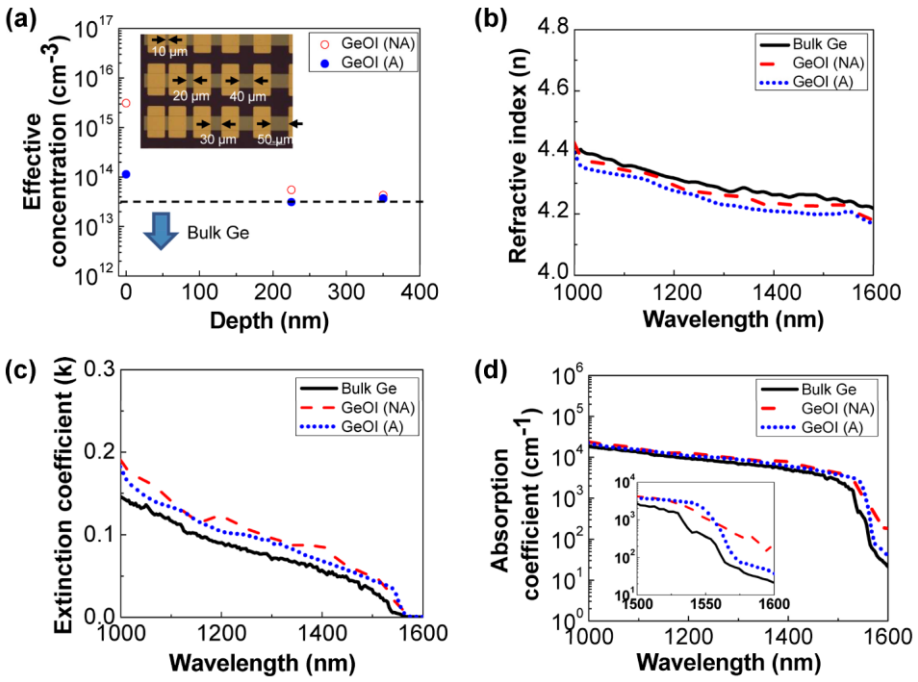

Fig. 3. (a) Measured free-carrier concentrations of Ge layers of non-annealed (NA) and annealed (A) GeOI wafers at 600˚C for 3 minutes. Inset shows a microscopic image of TLM patterns with various distances (i.e., 10, 20, 30, 40, and 50 μm) on Ge. Free-carrier concentration of bulk Ge wafer was presented for comparison. (b, c) Measured refractive indices and extinction coefficients of bulk Ge wafer and Ge layer of GeOI wafer in the case of NA and A at a wavelength range of 1000 ~1600 nm. (d) Absorption coefficient (α) of bulk Ge wafer and Ge layer of GeOI wafer calculated from the measured extinction coefficient (k) via $\alpha = 4\pi k/\lambda$. The inset shows magnified absorption coefficient spectra in a wavelength of 1500 ~1600 nm.

It is known that ion implantation can be used to manipulate optical and electrical properties of semiconductors [26,27]. Among various ions used for implantation, H + ions have been used for various applications, such as optical waveguide, electrical isolation, and semiconductor laser fabrication [28–30]. H implantation introduces high concentrations of vacancies in Ge. In addition, residual H + ions remain inside of the Ge layer of the GeOI wafer, as a result of H implantation when splitting the Ge layer from the bulk Ge wafer. The residual H + ions combine with these Ge vacancies to form V_2H with an acceptor energy level of 0.08 eV above the valence band of Ge [31]. A comparison of the free-carrier (hole) concentration, extracted from the TLM measurement results, is shown in Fig. 3(a). The free-carrier concentration of the Ge layer of the non-annealed (NA) GeOI wafer showed the highest value of 3×10^{15} cm^{-3} at the top surface of the Ge layer of the GeOI and is reduced to 5×10^{13} and 4×10^{13} cm^{-3} at the depth of 225 nm and 350 nm, respectively. In contrast, the free-carrier concentration in the Ge layer of the annealed GeOI wafer (1×10^{14} cm^{-3}) is lower by approximately an order of magnitude near the Ge top surface, although the free-carrier concentration eventually reached the similar values at the deeper regions. It should be noted that the measured free-carrier concentrations in the Ge layers of the GeOI wafers were greater than that of the bulk Ge wafer. The extra concentration of free carriers is ascribed to the electrically active acceptors that resulted from the residual H + . The higher free-carrier concentration near the top Ge surface (i.e., the deep regions of H implanted Ge wafer before splitting) of the GeOI wafer was observed, suggesting that the H distribution in the Ge layer is similar to the projected range (R_p) of the implanted H ions. A reduction of the free-carrier concentration can be largely attributed to recovered defects due to the thermal annealing.

Optics EXPRESS

In order to evaluate the changes of optical properties of H-implanted Ge layer of the GeOI wafer, refractive indices and extinction coefficients of bulk Ge wafer, non-annealed, and annealed GeOI wafers were carefully investigated using an ellipsometer (J. A. Woollam M-2000 DI) at a wavelength range of 1000 ~1600 nm. Figures 3(b)-3(c) show the refractive indices and extinction coefficients taken from the bulk Ge wafer, non-annealed, and annealed GeOI wafers, respectively. The refractive index and extinction coefficient of the Ge film of the GeOI wafers were fitted by considering the measured refractive index and extinction coefficient of the BOX layer in a fitting model (WVASE®) [32]. The measured refractive index of the bulk Ge wafer agreed well with the values reported elsewhere [33]. The Ge layer of the non-annealed GeOI wafer exhibited a slightly decreased refractive index with a Δn of 0.024, and that of the annealed GeOI wafer further decreased with a Δn of 0.046, compared to that of the bulk Ge wafer. In contrast, the extinction coefficient of the non-annealed GeOI wafer increased, with a Δk of 0.027 compared to that of the bulk Ge wafer over the measured wavelength range. The extinction coefficient of the annealed GeOI wafer slightly decreased, with a Δk of 0.008 compared to that of the non-annealed GeOI wafer. The trend in our experiment (i.e., decreased refractive index and increased extinction coefficient) was ascribed to the defects introduced by H + implantation. It should be noted that the effect of free-carrier concentration increase on the optical constants is negligibly small [34]. The absorption coefficient (α) of the Ge layer was calculated using the equation:

$$\alpha = (4 \times \pi \times k) / \lambda, \tag{1}$$

where α is the absorption coefficient, k the extinction coefficient, and λ the wavelength. As shown in Fig. 3(d), the absorption coefficient of the GeOI wafer increased compared to that of the bulk Ge wafer [9]. The non-annealed GeOI wafer showed a further enhanced absorption coefficient. It is noted that the absorption enhancement is more significant at longer wavelengths than the shorter ones. The absorption coefficients at 1600 nm increased from 22 cm^{-1} for the bulk Ge wafer to 40 and 224 cm^{-1} for the annealed and non-annealed GeOI wafers, respectively. It was reported that absorption coefficients of Ge on Si were approximately 500 and 900 cm^{-1} at 1600 nm by biaxial tensile strain of 0.2 and 0.25%, respectively [7]. It should be noted that our improvement in the absorption coefficient is not related to the tensile strain effect, as we confirmed it by Raman spectroscopy. Therefore, the absorption coefficient could be in fact further improved with the application of tensile strain [35].

To further verify the light absorption of the Ge NM, we performed reflection and transmission measurements on SU-8/PET and Ge NM/SU-8/PET stacks. The Ge NM (released) from the annealed GeOI wafer was used in this experiment. Figure 4(a) shows the microscopic image of the Ge NM/SU-8/PET stack. The size of the transferred Ge NM (i.e., 5 × 5 mm^2) was made to be larger than spot size of an incident light. The thicknesses of the Ge NM, SU-8, and PET were measured to be 0.4, 1, and 180 μm using a profilometer, respectively. Reflection and transmission spectra of the reference SU-8/PET structure were measured to be approximately 9.8% and 86% in average at the wavelength of 1000 ~1600 nm, respectively. In theory, the absorption (A) in the Ge layer can be calculated using the equation:

$$A = 1 - R - T, \tag{2}$$

where R and T refer to reflection and transmission, respectively [36]. The calculated absorption of 4.2% of the SU8/PET stack was not the ideal value, because absorption in the SU-8/PET stack was negligible, considering that the extinction coefficients of the SU-8 and PET are nearly zero in the near IR wavelength range. The possible, but negligible, measurement error could be from the scattering loss at the surface caused by non-ideal surface normal incidence.

Optics EXPRESS

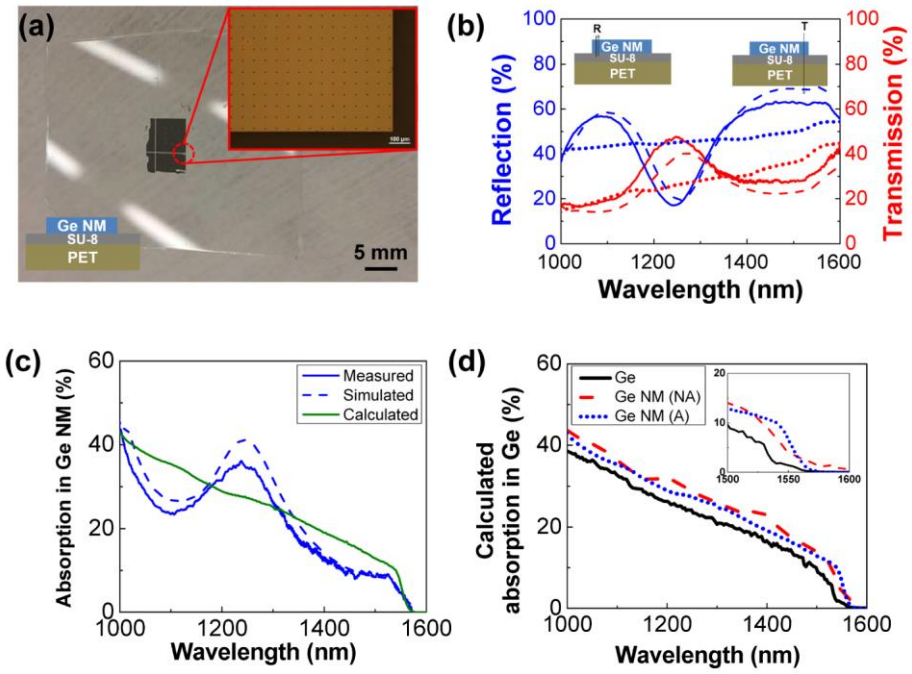

Fig. 4. (a) A microscopic image of the transferred Ge NM (size: 5 × 5 mm^2) on PET substrate. A bottom left inset shows a vertical layer structure of the sample and the top right inset shows the magnified image of the Ge NM. (b) Reflection and transmission spectra at a wavelength range of 1000 ~1600 nm. Note that the measured (solid line) and simulated (dashed line) spectra were obtained from Ge NM/SU-8/PET structure and calculated (dotted line) spectra came from the Ge NM. (c) Measured, simulated, and calculated absorption spectra of the Ge NM. (d) Comparison of the calculated absorption spectra from the Ge (not implanted) and Ge layer of GeOI wafer. Note that the same thickness of 400 nm was used. Inset shows magnified absorption spectra in a wavelength of 1500 ~1600 nm.

Figure 4(b) shows the reflection and transmission spectra of the Ge NM/SU-8/PET stack. The reflection was measured to be approximately 60% in the near IR range, except for the sharp drop near 1250 nm. Such optical characteristics can be ascribed to the Fabry-Perot oscillation due to finite thickness of PET substrate [37]. To accurately extract the absorption of the Ge NM from the measured reflection and transmission of the Ge NM/SU-8/PET stack, the following equation can be derived by considering the measurement error.

$$A_{Ge\,NM} = 1 - R_{Ge\,NM/SU-8/PET} - T_{Ge\,NM/SU-8/PET} - T_{Ge\,NM} \times E_{SU-8/PET}, \qquad (3)$$

where A is the absorption, R is the reflection, T is the transmission, and E is the measurement error. The measurement error (i.e., $E_{SU-8/PET}$) used in Eq. (3) refers to the value measured from the SU-8/PET stack. In the case of the Ge NM/SU-8/PET stack, the light that reaches the interface of the Ge NM and SU-8/PET will be T_{GeNM}, which should be incorporated in Eq. (3). To obtain the absorption ($A_{Ge\,NM}$) of the Ge NM, absorption of SU-8/PET should be subtracted from $A_{Ge\ NM/SU-8/PET}$ (1-$R_{Ge\ NM/SU-8/PET}$-$T_{Ge\ NM/SU-8/PET}$). Since the transmitted light ($T_{Ge\ NM}$) through the Ge NM is absorbed in the SU-8/PET, the absorption of the SU-8/PET can be calculated from $T_{Ge\ NM} \times A_{SU-8/PET}$ ($E_{SU-8/PET}$). Therefore, the absorption of the Ge NM can be calculated from the Eq. (3). Figure 4(c) shows the absorption spectrum of the Ge NM obtained by Eq. (3) in the wavelength range of 1000 ~1600 nm. The absorption gradually decreased from 44% at 1000 nm to 9% at 1526 nm, except for an abrupt increase of approximately 36% near 1240 nm. The absorption decreased sharply to 0% at 1572 nm, which agreed well with the measured extinction coefficient of Ge NM. The absorption coefficient of the annealed Ge NM was calculated to be 105 cm^{-1} at 1570 nm, and the

Optics EXPRESS

penetration depth was calculated to be 95 μm. There is no absorption at wavelengths larger than 1570 nm, which can be explained by the thinness (i.e., 400 nm) and penetration depth of the Ge NM.

To further compare the experimentally obtained spectra with theory and simulation, we obtained each spectrum using the following equations. Because the Ge NM is optically thin and polished, multiple reflections should be considered. The reflection, absorption, and transmission of the Ge NM were calculated numerically using the following equations [38].

$$r = \left[(n-1)^2 + k^2 \right] / \left[(n+1)^2 + k^2 \right], \tag{4}$$

$$R = r + \left[(1-r)^2 re^{-2\alpha t} / \left(1 - r^2 e^{-2\alpha t}\right) \right], \tag{5}$$

$$A = \left[(1-r)\left(1-e^{-\alpha t}\right) / \left(1 - re^{-\alpha t}\right) \right], \tag{6}$$

$$T = 1 - R - A, \tag{7}$$

where r is reflectivity, n is the refractive index, k is the extinction coefficient, α is the absorption coefficient, and t is the thickness. All parameters used in the calculation were the measured values. Besides the numerical calculation, a simulation was carried out using a three dimensional finite-difference time-domain (FDTD) software (Lumerical FDTD) to simulate the T, R, and A spectra. A vertically stacked structure of Ge NM/SU-8/PET with thicknesses of 0.4, 1, and 180 μm was used. Optical constants of the SU-8 and PET were taken from literature [39,40], while the optical constants of the Ge NM were based on the experimental data. The SU-8 and PET were assumed to be lossless in the simulation. As shown in Figs. 4(b)-4(c), good qualitative agreement was obtained among the measured, calculated, and simulated plot. It should be noted that an interference contrast was observed in experimental data due to multiple reflections inside the Ge NM/SU-8/PET stack.

Figure 4(d) shows comparative absorption spectra of the Ge (not H implanted), non-annealed, and annealed Ge NM in the same wavelength range. The absorption of Ge with the same thickness of 400 nm was calculated using the optical constants measured by the ellipsometer. The inset of Fig. 4(d) shows magnified spectra in the wavelength of 1500 ~1600 nm. It was observed that the absorptions of the non-annealed and annealed Ge NMs were slightly improved compared to that of the Ge across the measured wavelength. Zero absorption occurred at 1578 nm and beyond in the case of the Ge and the annealed Ge NM. However, the absorption of the non-annealed Ge NM extended to a longer wavelength, close to 1600 nm. In particular, the non-annealed Ge NM showed 0.8% of the absorption even at 1600 nm.

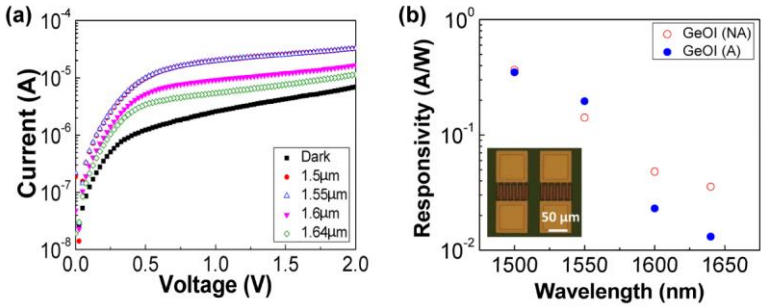

Fig. 5. (a) Measured I-V characteristics from MSM photodetector fabricated on non-annealed GeOI. (b) Measured responsivity spectra of the MSM Ge NM-based photodetectors using the non-annealed (NA) and annealed (A) GeOI wafers at a wavelength range of 1.5 ~1.64 μm with a wavelength step of 50 nm. Inset shows a microscopic image of the fabricated MSM photodetectors.

Optics EXPRESS

MSM Ge NM-based photodetectors were fabricated using non-annealed and annealed GeOI wafers. Figure 5(a) shows the measured I-V characteristics of MSM photodetectors fabricated on the non-annealed GeOI under various wavelengths. Figure 5(b) shows a comparison of typical responsivity spectra of the photodetectors at 2 V bias. Responsivity of the device with non-annealed Ge NM was constantly higher than that of the device with annealed Ge NM under near IR illumination, except for that at 1550 nm. The responsivity at 1600 and 1640 nm increased from 0.023 A/W and 0.013 A/W to 0.048 A/W and 0.036 A/W, respectively. The enhanced responsivity of non-annealed cases at 1500, 1600, 1640 nm was consistent with the absorption spectra of the Ge NM as shown in Fig. 4(d). Although the responsivity may not be sufficient for commercial applications, it can be improved using thicker Ge layer [41]. Reflection techniques such as a distributed Bragg reflector (DBR) and a back-side metal reflector can further enhance the responsivity [9,18]. It should be noted that the measured dark current of the device with the non-annealed Ge NM was 6.95 μA, which was higher than the annealed case (4.84 μA) at 2 V bias. This agreed well with the larger free-carrier concentration of the non-annealed Ge NM since the free carriers contribute to electrical conductivity. Overall, the improved photo-responsivity of the Ge photodetector might be attributed to enhanced absorption in Ge NM using H ion implantation.

4. Conclusion

In summary, we have demonstrated that the use of H ion implantation can enhance light absorption in Ge to extend its useful wavelength range for photon detection. The refractive index of the Ge layer of the GeOI wafer after H + ion implantation decreased with a Δn of 0.024, while the extinction coefficient increased with a Δk of 0.027 compared to those of the bulk Ge wafer at the wavelength range of 1000 ~1600 nm, respectively. Although annealing further decreased the refractive index with an additional Δn of 0.022, it slightly decreased the extinction coefficient, having a Δk of 0.008 compared to that of the Ge layer of non-annealed GeOI wafer. Based on the measured optical constants, the absorption coefficient of the non-annealed GeOI wafer was calculated to be 224 cm^{-1} at 1600 nm, 10 times larger than that of the bulk Ge wafer (i.e., 22 cm^{-1}) and about 5 times larger than that of the annealed GeOI wafer (i.e., 40 cm^{-1}). The enhanced light absorption of H implanted Ge was further characterized on transferred Ge NMs on PET substrates. Absorption of the bulk Ge wafer and annealed Ge NM with the same thickness of 400 nm dropped to zero at 1578 nm, whereas absorption wavelength of the non-annealed Ge NM was extended over 1600 nm. The measured responsivity spectra of Ge photodetectors exhibited the same behavior as the absorption spectra of the Ge NMs.

Acknowledgements

This work is supported by AFOSR under a PECASE grant # FA9550-09-1-0482. The program manager is Dr. Gernot Pomrenke.